

LTCC VERTICALLY-STACKED CROSS-COUPLED BAND-PASS FILTER FOR LMDS BAND APPLICATIONS

K.-S. Chin^{*}, C.-H. Chen, and C.-C. Chang

Chang Gung University, Taoyuan 333, Taiwan, R.O.C.

Abstract—This study develops a compact 28 GHz bandpass filter on a low-temperature co-fired ceramic substrate for applications in LMDS (Local Multipoint Distribution Service) bands. The filter comprises two pairs of vertically stacked cross-coupled open loops with vertical interconnection structures, achieving compactness, high integration, and superior frequency selectivity. Attaining selective response with two transmission zeros requires adjusting the couplings of adjacent resonators and external quality factor. The open loops are fed by using the three-via vertical interconnections to prevent any electrical effect on the filter. Measurements correlate closely with the simulation results: this study achieved a bandwidth of 2.1 GHz (27.6–29.7 GHz) with two zeros located at 25.8 GHz and 31.1 GHz, and a compact size of $2.69 \times 2.66 \times 0.4 \text{ mm}^3$.

1. INTRODUCTION

LMDS (Local Multipoint Distribution Service) is a novel wireless communication technology that shows considerable promise. LMDS uses Ka-band signals such as 27.5–28.35 GHz, 29.1–29.25 GHz, 31.075–31.225 GHz, 31–31.075 GHz, and 31.225–31.3 GHz to send voice, video, and data at 1 Gbps or more [1–3]. Ka-band bandpass filters are necessary for LMDS communication systems. Due to their extremely short wavelengths, Ka-band signals require accurate circuit dimensions to achieve high electrical performance, raising the difficulty in filter design and fabrication. The recent implementation of a 3D-structure filter has become popular for its compactness and high integration, which requires filters to be embedded, stacked, and folded with a multilayer configuration. However, connecting the cross-layer resonators without hindering their performance is difficult, especially

Received 11 May 2011, Accepted 16 June 2011, Scheduled 22 June 2011

* Corresponding author: Kuo-Sheng Chin (kschin@mail.cgu.edu.tw).

at high frequencies. Superior circuit structure and fabrication process are still challenging for Ka-band filter design.

Cross-coupled filters are favored for their planar, light weight, and ease of manufacture in low frequency bands, which enhances their practicality. The cross-coupled structure typically comprises four resonators to establish two signal propagation paths. When the cross coupling path is out of phase with the main path coupling, a pair of transmission zeros can be created at the skirt of the passband to improve frequency selectivity. Numerous studies have emphasized the improvement of cross-coupled filters [4–15, 17] and direct-coupled filters [16, 18]. In one investigation [4], the high-temperature superconductor films were used to design fourth-order open-loop filters with low insertion loss. Two pairs of transmission zeros were created via skew-symmetric feeding of the filter. Tang [5] utilized a hybrid structure of microstrips associated with lumped elements in low-temperature co-fired ceramic (LTCC) fabrication, and coupled the input and output ports, increasing a pair of zeros. However, more metal layers are required for this design. Lin et al. proposed a design method for inducing self coupling in resonators of cross-coupled filters [6]. The asynchronously tuned resonators have different resonant frequencies performing a single zero at the single side of a passband. However, the coupling coefficient is difficult to extract. One study [7] presented a three cross-coupled structure and frequency transformation from a lowpass response to a triple-band bandpass response, synthesizing triple-band filters with a pair of zeros for each band.

Another investigation [8] developed a novel $\lambda/4$ stepped-impedance resonator with several grounded strips in a low-impedance section to design cross-coupled filters, achieving high circuit fabrication tolerance. A cross-coupled dual-band filter with four equal length split-ring resonators was designed in [9] for size reduction. In [10], the stepped-impedance open-loop resonator on CMOS fabrication was adopted to realize filters; the center frequency can rise up to 58–66.5 GHz, though with a large insertion loss of 5.9 dB. Most of the aforementioned approaches are presented in low-frequency bands, and less are in Ka-bands due to the difficulty of achieving high frequency. The large size of cross-coupled resonator filters is also a major disadvantage. Thus, the design of a low insertion loss, small size, high selectivity, and easy fabrication cross-coupled filter realized at a millimeter wave frequency is an ongoing challenge.

In recent years, LTCC has become an attractive fabrication process particularly effective for use in high-frequency circuits. This work presents a feasible design of vertically-stacked cross-coupled filters

for LMDS band applications. Two pairs of open-loop resonators are embedded and vertically stacked using LTCC multilayer structure to reduce size significantly. The total size of this experimental filter is only $2.69 \times 2.66 \times 0.4 \text{ mm}^3$. Embedded multilayer filter configuration also provides another dimension in the flexible design and integration of other microwave circuits, which is often needed in System-in-Package (SiP) approach. For operation at LMDS band, two superior vertical interconnection structures are developed to draw out the embedded I/O feed lines for connection, ensuring excellent signal transmission at high frequency of up to 37 GHz. An experimental LTCC filter was fabricated for demonstration. Measured results show a bandwidth of 7.4% and a low insertion loss of 3.2 dB, with a pair of transmission zeros at the band edges. The proposed cross coupled filter can be produced with more consistently stable performance, of which the required fabrication accuracy ($\geq 0.1 \text{ mm}$) is very easy to achieve using the general LTCC fabrication process.

2. COUPLING COEFFICIENT AND EXTERNAL QUALITY FACTOR

For compactness, the half-wavelength open-loop microstrips with $\lambda_g/2 = 2(X+Y-2W)-g$ are adopted as resonators, as shown in Fig. 1, where λ_g is the guided wavelength. Fig. 2(a) plots the conventional fourth-order bandpass filter with four coplanar $\lambda_g/2$ open loops. This cross-coupled structure establishes two coupling paths, 1-2-3-4 and 1-4, creating a pair of transmission zeros located at the two edges of the passband, improving frequency selectivity significantly. This type of filter is also called a selective-response filter. For further size reduction, the single-layered structure can be modified into a multilayer structure, as shown in Fig. 2(b), in which two pairs of embedded $\lambda_g/2$ open loops are stacked vertically, with a common ground placed in-between. Two rectangular apertures are etched in the ground to provide adequate

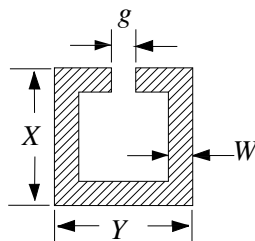


Figure 1. Half-wavelength open-loop microstrip resonator.

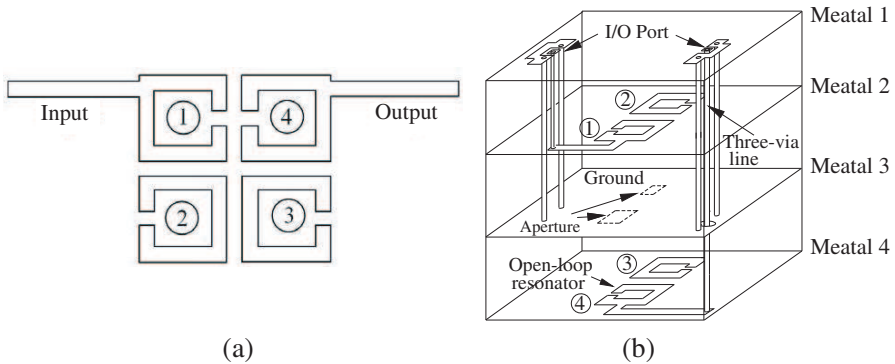


Figure 2. (a) Conventional planar cross-coupled open-loop bandpass filter. (b) Proposed vertically-stacked cross-coupled open-loop bandpass filter.

coupling between resonators, while the signal via can pass through a circular aperture. A novel three-via vertical interconnection structure is also developed for feeding signals into and out of the filter.

Because the length of the resonator ($\lambda_g/2$) is extremely short at such a high Ka-band (typically < 2 mm), a ratio of line width/loop length = $1/5$ is required for folding the shape of resonators adequately to be a square open loop. The area enclosed by the loop also requires careful design. Fig. 3 is an inadequate example of having excessive line width and a small enclosed area of loops, which renders its shape more akin to parallel-coupled lines with connected ends, resulting in deviated resonant characteristics. A narrower line width is preferred for folding microstrip lines to form a loop with ease. The line width is generally limited by the circuit accuracy and thickness of ceramic layers, specified according to LTCC design rules. A higher dielectric constant of LTCC is superior because the line width is inversely proportional to the dielectric constant for fixed impedance. If a dielectric constant $\epsilon_r = 7.5$, loss tangent = 0.005, and a substrate thickness of 0.1 mm are adopted, the dimensions of the $\lambda_g/2$ open loop are $X = 0.62$ mm, $Y = 0.62$ mm, $W = 0.1$ mm, and $g = 0.1$ mm.

Figure 4 shows the equivalent circuit of the proposed cross-coupled bandpass filter, where $\omega_o = (L_i C_i)^{-1/2}$ is the resonant angular frequency. The coefficients K_{ij} specify the coupling between adjacent resonators i and j of the filter. Q_{ei} and Q_{eo} are the external quality factors that specify the input and output couplings, respectively. K_{ij} and Q_e can be determined from the associated low-pass prototype filter. When choosing a selective-response with

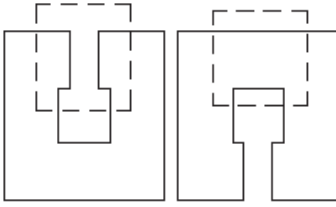


Figure 3. Inadequate example of designing $\lambda_g/2$ open-loop resonators.

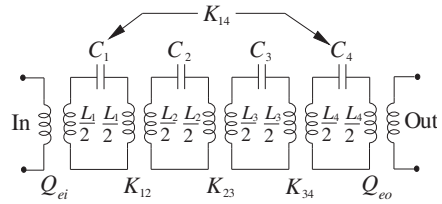


Figure 4. Equivalent circuit of the cross-coupled bandpass filter.

a fourth-order, fractional bandwidth of 8%, return loss of 20 dB, and a normalized frequency of transmission zeros $\Omega_a = 2.2$, the element values g_i of a low-pass prototype filter and the admittance inverter J_i can be calculated from (1)–(4) [14], obtained as $g_0 = 1$, $g_1 = 0.95063$, $g_2 = 1.35908$, $J_1 = -0.12992$, and $J_2 = 1.02499$.

$$g_1(\Omega_a) = 1.22147 - 0.35543\Omega_a + 0.18337\Omega_a^2 - 0.0447\Omega_a^3 + 0.00425\Omega_a^4 \quad (1)$$

$$g_2(\Omega_a) = 7.22106 - 9.48678\Omega_a + 5.89032\Omega_a^2 - 1.65776\Omega_a^3 + 0.17723\Omega_a^4 \quad (2)$$

$$J_1(\Omega_a) = -4.30192 + 6.26745\Omega_a - 3.67345\Omega_a^2 + 0.9936\Omega_a^3 - 0.10317\Omega_a^4 \quad (3)$$

$$J_2(\Omega_a) = 8.17573 - 11.36315\Omega_a + 6.96223\Omega_a^2 - 1.94244\Omega_a^3 + 0.20636\Omega_a^4 \quad (4)$$

$$K_{1,2} = K_{3,4} = \frac{FBW}{\sqrt{g_1 g_2}} \quad (5)$$

$$K_{1,4} = \frac{FBW \cdot J_1}{g_1} \quad (6)$$

$$K_{2,3} = \frac{FBW \cdot J_2}{g_2} \quad (7)$$

$$Q_{ei} = Q_{eo} = \frac{g_0 g_1}{FBW} \quad (8)$$

Substituting g_i and J_i into (5)–(8) yields $K_{12} = K_{34} = 0.0704$, $K_{14} = -0.0109$, $K_{23} = 0.0603$, and $Q_{ei} = Q_{eo} = 11.883$. These results shows that the coupling coefficients of K_{12} , K_{23} , and K_{34} should be realized with magnetic or mixed coupling since their values are positive, while K_{14} necessitates the use of electric coupling because a negative value is required. As shown in Fig. 2, the electric coupling coefficient K_{14} requires that the open sides of resonators 1 and 4 are proximately placed to perform the coupling of electric fringe fields, and the magnetic coupling coefficient K_{23} requires the back sides of resonators 2 and 3 having stronger magnetic fringe fields to be proximately placed.

The design curves of coupling coefficients are necessary for adjusting the proper couplings between resonators to match the desired filter response. Figs. 5–7 plot the simulated coupling coefficients K_{14} (electric coupling), K_{23} (magnetic coupling), and K_{12} (mixed coupling, $K_{34} = K_{12}$) of coupled open-loop pairs versus the aperture widths Y_1 , Y_2 , and the gap S , respectively. Fig. 8 shows the external quality factor Q_e versus the feeding position t with taped input.

Notably, an appropriate arrangement of resonator positions can avoid re-extraction of coupling coefficients when filter specifications are changed. Fig. 9(a) shows an inadequate arrangement of resonators, in which the resonators 1 and 4 are placed on top layer and resonators 2 and 3 are located on bottom layer with a common ground plane in between. K_{14} and K_{23} respectively use gaps S_{14} and S_{23} to control

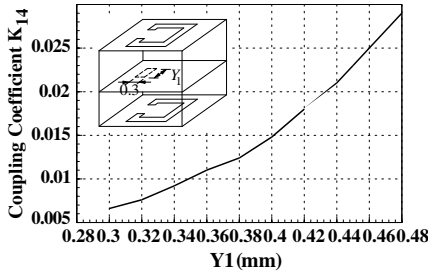


Figure 5. The electric coupling coefficient K_{14} versus the aperture width Y_1 with a fixed aperture length of 0.3 mm.

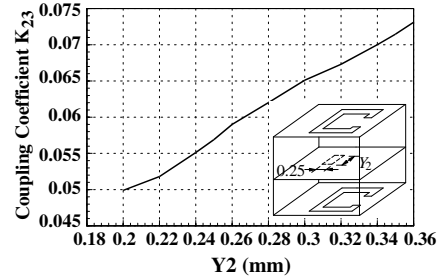


Figure 6. The magnetic coupling coefficient K_{23} versus the aperture width Y_2 with a fixed aperture length of 0.25 mm.

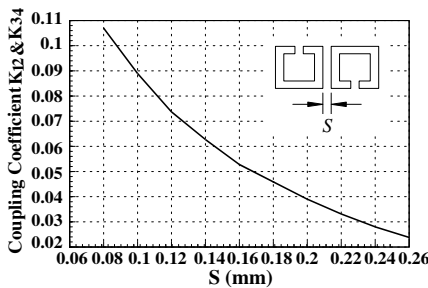


Figure 7. The mixed coupling coefficients K_{12} and K_{34} versus the gap S .

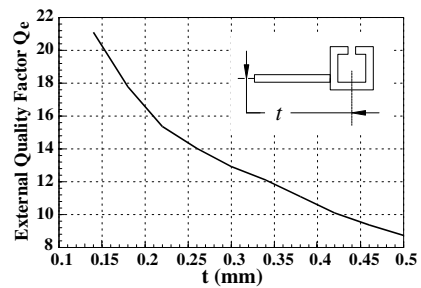


Figure 8. The external quality factor Q_e versus the feeding position t with taped input.

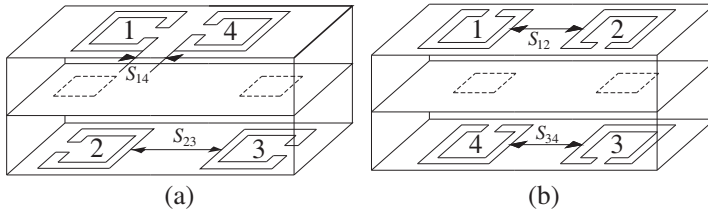


Figure 9. (a) Cross-sectional configuration of an inadequate arrangement of resonators. (b) The proposed arrangement of resonators.

their coupling coefficients. As aforementioned, $K_{14} \neq K_{23}$ specified by filter specifications, thus the positions of resonators 1 and 2 (and also positions of resonators 3 and 4) are not vertically aligned because of $S_{14} \neq S_{23}$. K_{12} and K_{34} are controlled by the two ground apertures which should locate according the relative positions of resonators 1 and 2 and positions of resonators 3 and 4, respectively, ensuring all four coupling coefficients are fulfilled simultaneously. When the filter specifications are given, K_{14} and K_{23} should design first to obtain the required gaps of S_{14} and S_{23} . After all positions of resonators are fully determined, then ground apertures can be set to establish the design curves of K_{12} and K_{34} by adjusting the size of apertures. Therefore, K_{12} and K_{34} can not be decided independently without considering the relative positions of horizontally adjacent resonators. In other words, K_{12} and K_{34} are calculated only for specific values of K_{14} and K_{23} . Once the filter specifications are changed, the design curves of K_{12} and K_{34} should be re-established according the changed spacing of S_{14} and S_{23} , which is not convenient for filter design.

Figure 9(b) shows the proposed resonator arrangement, where the resonators 1 and 2 are placed on top layer and resonators 3 and 4 are located on bottom layer. Since K_{12} and K_{34} are identical, they have the same gaps ($S_{12} = S_{34}$). Therefore, resonators 1 and 4, and resonators 2 and 3, are vertically aligned, respectively. The ground apertures of K_{14} and K_{23} are placed between the open sides of loops 1 and 4 and the back sides of loops 2 and 3, respectively. Both K_{14} and K_{23} can be extracted independently regardless of the relative positions of horizontally adjacent resonators. The proposed resonator arrangement is more convenient for extraction of K_{14} and K_{23} . Even the filter specifications are changed, the design curves of K_{14} and K_{23} do not require to be re-established.

3. LTCC VERTICAL INTERCONNECTION STRUCTURE

Feeding a Ka-band cross-layer signal into and out of embedded resonators without disturbing their performance is difficult. Vertical interconnection is essential for providing superior frequency response, ensuring good signal transmission between cross-layer connections. Signal vias are often used in interconnection structures, though vias can potentially cause serious parasitic inductance behaving similarly to low-pass filters and attenuating high-frequency components [19–24]. A sound vertical interconnection structure should have a lower insertion loss and a higher return loss within the operation band. This study constructs a vertical three-via (ground-signal-ground) interconnection demonstrating an excellent S -parameter performance of up to 37 GHz.

Figure 10(a) shows the three dimensions of an LTCC vertical interconnection configuration for the input RF-probing pad and Resonator 1, allowing ease of on-chip measurement. The 250 μm pitch is designed for RF probing. Fig. 10(a) shows that three vias (one signal via and two ground vias) and three metal layers are used in the design, in which the input port and Resonator 1 are situated on the different layers above the ground plane. The two ground pads are connected further to form a guard ring for equalizing the ground potential and providing excellent RF shielding at high frequencies. The diameter of vias is $d = 0.1\text{ mm}$, and ground vias are placed at both sides of the signal via with a spacing of $w = 0.36\text{ mm}$. The proposed vertical interconnection structure smoothes the field transformation of the LTCC cross-layer connection providing good circuit performance at high frequencies. Fig. 10(b) displays another feeding structure for Resonator 4 to be exit the output port. The RF-probing pad and

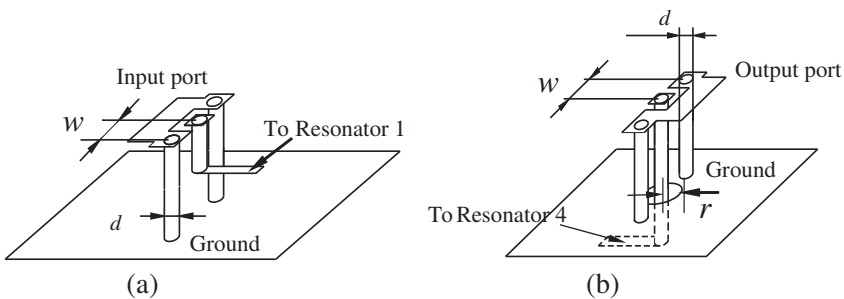


Figure 10. (a) Vertical interconnection for input RF-probing pad and Resonator 1. (b) Vertical interconnection for Resonator 4 to the output port.

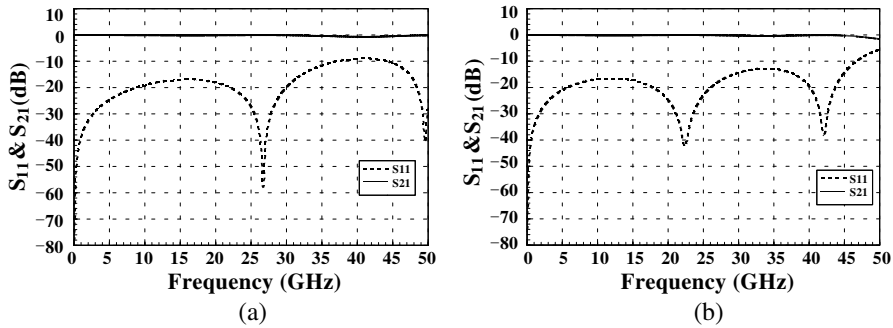


Figure 11. (a) Simulated S parameters of the vertical interconnection in Fig. 10(a). (b) Simulated S parameters of Fig. 10(b).

Resonator 4 are situated on a different side of the ground plane. The signal via can pass through an etched circular ground aperture with a radius of $r = 0.2$ mm. The proposed structure can also be applied for any embedded circuit measurement requiring an RF signal fed and received by G-S-G pads.

Figures 11(a) and (b) are the simulated S -parameter responses of the proposed vertical interconnection in Figs. 10(a) and (b), respectively, by regarding them as two-port networks, with an excellent performance of $|S_{11}| > 10$ dB and $|S_{21}| < 0.48$ dB of up to 37 GHz.

4. ILLUSTRATED EXAMPLE OF THE LTCC 28 GHz BANDPASS FILTER

A vertically-stacked cross-coupled bandpass filter operating at 28 GHz was synthesized on an LTCC substrate to validate the design approach. Specifications of this filter are chosen as a selective response, $N = 4$, $FBW = 8\%$, a return loss of 20 dB, and $\Omega_a = 2.2$. The associated coupling coefficients and external quality factors have been calculated, as seen in Section 2. The LTCC material system with a relative permittivity of 7.5 and a loss tangent of 0.005 was utilized. The design comprises four ceramic layers and four metals with silver conductor metalization and via metal. Each ceramic layer has a thin thickness of 0.1 mm reducing the parasitic via inductance as much as possible and narrowing the line width to fold the shape of square loops adequately. The full-wave electromagnetic simulator Ansoft HFSS was used for the simulation.

The required coupling coefficients and external quality factors can be achieved according to the design curves from Figs. 5–8. The aperture size for the electric coupling K_{14} is 0.36×0.3 mm² ($Y_1 =$

0.36 mm) and the magnetic coupling K_{23} is $0.27 \times 0.25 \text{ mm}^2$ ($Y_2 = 0.27 \text{ mm}$). The gap for mixed couplings K_{12} and K_{34} require that $S = 0.12 \text{ mm}$, and for Q_e necessitates that $t = 0.35 \text{ mm}$. Upon optimization, Y_1 , Y_2 , S , and t are adjusted slightly to 0.45 mm, 0.25 mm, 0.08 mm, and 0.44 mm, respectively, for optimal filter performance. Table 1 lists the physical dimensions. Fig. 12 displays the photos of the experimental vertically-stacked cross-coupled filter, in which the photo of each layer is contrasted with a 3D configuration of the filter.

Table 1. Circuit dimensions (in mm) of the experimental filter.

Open-loop resonator		Coupling aperture (K_{14})		Coupling aperture (K_{23})		Thickness of LTCC substrate
Length	Width	Length	Width	Length	Width	
0.62	0.62	0.45	0.3	0.25	0.25	0.1
Spacing of loops (K_{12} and K_{34})		Position of taped input/output line		Width of taped line (50 Ω)		Radius of circular ground aperture
$S = 0.08$		$t = 0.44$		0.1		0.2
Via diameter		Spacing of vias		Pitch of pads		Total filter size
0.1		0.36		0.25		$2.69 \times 2.66 \times 0.4$

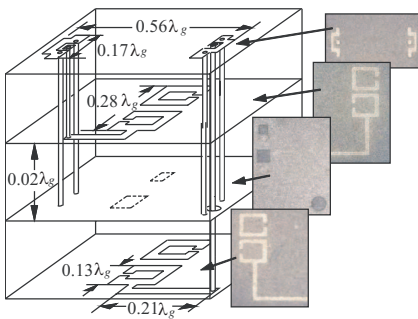


Figure 12. Photo of the proposed 28 GHz LTCC vertically-stacked cross-coupled bandpass filter.

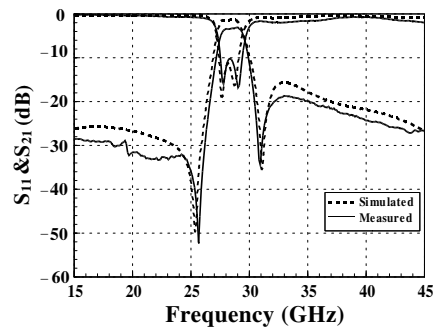


Figure 13. The simulated and measured S -parameter responses of the experimental LTCC 28 GHz bandpass filter.

The prototype S parameters were measured using RF probes and an Agilent E8364C network analyzer with SOLT calibration. Fig. 13 shows the simulated and measured S -parameter responses, and both results are in sound agreement. The measurements results reveal that the central frequency shifted to 28.5 GHz slightly with a bandwidth of 7.4% (27.6–29.7 GHz). The insertion loss is lower than 3.2 dB and the return loss is greater than 10 dB. As this figure shows, two transmission zeros are located at 25.8 and 31.1 GHz, resulting in excellent frequency selectivity. The size of this filter is approximately $2.69 \times 2.66 \times 0.4 \text{ mm}^3$, including I/O pads, which is extremely compact, owing to its vertically-stacked structure.

5. CONCLUSION

This study designed an LTCC 28 GHz cross-coupled bandpass filter for LMDS applications. Such a high-frequency filter is a challenge requiring extreme fabrication accuracy. The proposed filter structure comprises two pairs of vertically-stacked half-wavelength open loops on an LTCC substrate to reduce the size significantly. Two coupling paths are formed to create a pair of transmission zeros at the band edges, to raise frequency selectivity. Filter response is synthesized by adjusting the coupling coefficients of the adjacent resonators and external quality factors. This study also developed two novel vertical interconnection structures for cross-layer connections. The design concept was demonstrated by fabricating an experimental 28 GHz bandpass filter that yielded a bandwidth of 7.4% and a low insertion loss of 3.2 dB.

ACKNOWLEDGMENT

This work was partially supported by the National Science Council, Taiwan, R.O.C., (NSC 99-2221-E-182-033) and Chang Gung University, Taiwan, R.O.C., (UERPD290051). The authors would also like to acknowledge the support of High Speed Intelligent Communication (HSIC) Research Center and Healthy Aging Research Center (HARC), Chang Gung University.

REFERENCES

1. Chen, K.-S. and C.-Y. Chu, "A propagation study of the 28 GHz LMDS system performance with M-QAM modulations under rain fading," *Progress In Electromagnetics Research*, Vol. 68, 35–51, 2007.

2. Kulke, R., G. Möllenbeck, W. Simon, A. Lauer, and M. Rittweger, "Point-to-multipoint transceiver in LTCC for 26 GHz," *IMAPS-Nordic*, 50–53, Stockholm, 2002.
3. Chin, K.-S., H.-T. Chang, J.-A. Liu, B.-G. Chen, J.-C. Cheng, and J. S. Fu, "Stacked patch antenna array on LTCC substrate operated at 28 GHz," *Journal of Electromagnetic Waves and Applications*, Vol. 25, No. 4, 527–538, 2011.
4. Wang, L.-M., et al., "Cross-coupled YBCO filters with spurious suppression using tap-connection technique and skew-symmetric feeds," *IEEE Trans. Applied Superconductivity*, Vol. 17, 894–897, Jun. 2007.
5. Tang, C.-W., "Design of four-ordered cross-coupled bandpass filters with low-temperature co-fired ceramic technology," *IET Microw. Antennas Propag.*, Vol. 3, 402–409, 2009.
6. Lin, C.-H., C.-H. Wang, and C.-H. Chen, "A simple design procedure for the asynchronous box-section filter," *Asia-Pacific Microwave Conference Proceedings*, 807–810, Thailand, 2007.
7. Di, H., B. Wu, X. Lai, and C.-H. Liang, "Synthesis of cross-coupled triple-passband filters based on frequency transformation," *IEEE Microwave and Wireless Components Letters*, Vol. 20, No. 8, 432–434, Aug. 2010.
8. Liang, C.-H., C.-H. Chen, and C.-Y. Chang, "Fabrication-tolerant microstrip quarter-wave stepped-impedance resonator filter," *IEEE Trans. Microwave Theory Tech.*, Vol. 57, 1163–1172, May 2009.
9. Fan, J.-W., C.-H. Liang, and X.-W. Dai, "Design of cross-coupled dual-band filter with equal-length split-ring resonators," *Progress In Electromagnetics Research*, Vol. 75, 285–293, 2007.
10. Yang, B., E. Skafidas, and R. J. Evans, "60 GHz compact integrated cross-coupled SIR-MH bandpass filter on bulk CMOS," *Electronics Letters*, Vol. 44, No. 12, 738–740, Jun. 2008.
11. Kuo, J.-T., S.-C. Tang, and S.-H. Lin, "Quasi-elliptic function bandpass filter with upper stopband extension and high rejection level using cross-coupled stepped-impedance resonators," *Progress In Electromagnetics Research*, Vol. 114, 395–405, 2011.
12. Zhan, J.-S. and J.-L. Wang, "A simple four-order cross-coupled filter with three transmission zeros," *Progress In Electromagnetics Research C*, Vol. 8, 57–68, 2009.
13. Wang, Z., S. Bu, and Z.-X. Luo, "A Ka-band third-order cross-coupled substrate integrated waveguide bandpass filter base on 3D LTCC," *Progress In Electromagnetics Research C*, Vol. 17, 173–

- 180, 2010.
14. Hong, J.-S. and M. J. Lancaster, *Microstrip Filters for RF/Microwave Application Engineering*, John Wiley & Sons, New York, 2001.
 15. Chin, K.-S. and D.-J. Chen, "Harmonic-suppressing bandpass filter based on coupled triangular open-loop stepped-impedance resonators," *Microw. Optical Tech. Lett.*, Vol. 52, No. 1, 187–191, Jan. 2010.
 16. Chin, K.-S. and D.-J. Chen, "Novel microstrip bandpass filters using direct-coupled triangular stepped-impedance resonators for spurious suppression," *Progress In Electromagnetics Research Letters*, Vol. 12, 11–20, 2009.
 17. Wen, S. and L. Zhu, "Numerical synthesis design of coupled resonator filters," *Progress In Electromagnetics Research*, Vol. 92, 333–346, 2009.
 18. Xiao, J.-K. and Y. Li, "Novel compact microstrip square ring bandpass filters," *Journal of Electromagnetic Waves and Applications*, Vol. 20, No. 13, 1817–1826, 2006.
 19. Wang, Z., X. Zeng, B. Yan, R. Xu, and W. Lin, "A millimeter-wave *E*-plane band-pass filter using multilayer low temperature co-fired ceramic (LTCC) technology," *Journal of Electromagnetic Waves and Applications*, Vol. 24, No. 1, 71–79, 2010.
 20. Panther, A., C. Glaser, M. G. Stubbs, and J. S. Wight, "Vertical transitions in low temperature co-fired ceramics for LMDS applications," *IEEE MTT-S Int Microwave Symp Dig.*, 1907–1910, 2001.
 21. Valois, R., D. Baillargeat, S. Verdeyme, M. Lahti, and T. Jaakola, "High performance of shielded LTCC vertical transitions from DC up to 50 GHz," *IEEE Trans. Microwave Theory Tech.*, Vol. 53, 2026–2032, 2005.
 22. Stark, A. and A. F. Jacob, "A broadband vertical transition for millimeter-wave applications," *Proceedings of the 38th European Microwave Conference*, 476–479, 2008.
 23. Stark, A., H. Olbert, and A. F. Jacob, "Defected and floating ground structures for vertical interconnects," *Proceedings of the 39th European Microwave Conference*, 153–156, 2009.
 24. Xia, L., R.-M. Xu, and B. Yan, "LTCC interconnect modeling by support vector regression," *Progress In Electromagnetics Research*, Vol. 69, 67–75, 2007.